

Effect of temperature on straining of AISI 304 austenitic stainless steel

ABSTRACT

The study examined the influence of plastic strain on AISI 304 austenitic stainless steel at room (298 K) and cryogenic (93 K) temperatures. Initially, seven samples were performed in different levels of engineering strain (0.125, 0.25, 0.375, 0.5, 0.625, 0.75, 0.875 mm/mm) at both temperatures. Their results were compared to an as-received undeformed sample, and the analysis of the microstructure evolution involved techniques such as optical microscopy, microhardness measurements, and ferritescopy. Subsequently, complete mechanical tests were conducted until the sample failed at each temperature, generating stress-strain curves. These experiments were performed using the Thermomechanical Simulation System (XTMS) located at the XRD1 experimental station within the National Synchrotron Light Laboratory (LNLS) at the National Center for Research in Energy and Materials (CNPEM). The findings indicated that the quantity of strain-induced martensite α' (SIM- α') increased with the strain level, particularly in samples performed at low temperatures. At an engineering strain of 0.875 mm/mm, the amount of SIM- α' reached 96% at 93 K, whereas it only reached 60% at room temperature under the same conditions. Additionally, cryogenic straining resulted in higher transformation rates of SIM- α' and greater microhardness values. Moreover, cryogenic straining led to a significant increase in yield strength (205% higher) and tensile strength (96% higher), with a minimal decrease in uniform elongation (4.3% less) compared with room temperature straining. These effects were attributed to the partial suppression of dynamic recovery and the transformation of austenite into SIM- α' . The results suggest the occurrence of the Transformation Induced Plasticity (TRIP) effect, contributing to the improvement of mechanical strength. This study demonstrated that straining at cryogenic temperatures induces favorable changes in the mechanical properties of austenitic stainless steel by transforming austenite into SIM- α' and inhibiting dynamic recovery.

KEYWORDS: stress-strain; austenite; strain-induced martensite.

Denilson José Marcolino de

Aguiar

denilsonaguaiar@utfpr.edu.br

orcid.org/0000-0001-7253-9193

Universidade Tecnológica Federal do Paraná, Ponta Grossa, Brasil.

Henry Otávio Fontana

henryfontana@alunos.utfpr.edu.br

orcid.org/0000-0002-3731-1676

Universidade Tecnológica Federal do Paraná, Ponta Grossa, Brasil.

Deize Basílio dos Santos de

Aguiar

deizebasilio@gmail.com

orcid.org/0000-0002-2059-6871

Faculdade Cesumar, Ponta Grossa, Paraná, Brasil.

Ana Luisa Terasawa Senra

ana.terasawasenra@gmail.com

orcid.org/0000-0002-8749-8192

Universidade Estadual de Ponta Grossa, Ponta Grossa, Paraná, Brasil.

Marcel Tadashi Izumi

marcel.izumi@gmail.com

orcid.org/0000-0002-5171-8413

Universidade Estadual de Ponta Grossa, Ponta Grossa, Paraná, Brasil.

Leonardo Wu

leonardo.wu@lnls.br

orcid.org/0000-0003-3298-8589

Centro Nacional de Pesquisa em Energia e Materiais, Campinas, São Paulo, Brasil.

Alexandre Magnus Gomes

Carvalho

amgcarvalho80@gmail.com

orcid.org/0000-0001-6439-414X

Universidade Estadual de Maringá, Maringá, Paraná, Brasil.

Oswaldo Mitsuyuki Cintho

omcyntho@uepg.br

orcid.org/0000-0001-8567-5653

Universidade Estadual de Ponta Grossa, Ponta Grossa, Paraná, Brasil.

INTRODUCTION

Austenitic stainless steels are widely recognized for their appreciable yield strength, tensile strength, uniform elongation, and high corrosion resistance in several corrosive environments. The primary phase in this category of steels is austenite, characterized by a face-centered cubic crystal structure (FCC), paramagnetic behavior (CELADA-CASERO *et al.*, 2017), and potential residual fractions of δ -ferrite (MAXIMOV *et al.*, 2023) or SIM- α' by straining during the manufacturing process, which may persist even after heat treatments. The chemical composition of these steels typically includes significant concentrations of chromium (16%-30%) and nickel (8%-20%), along with potential alloying elements such as molybdenum and titanium, to achieve specific properties. Nickel stabilizes the austenite phase, while chromium stabilizes the ferrite phase. Among these steels, AISI 304 austenitic stainless steel is widely utilized, although grades like AISI 316 offer superior corrosion resistance due to molybdenum (CRIVOI *et al.*, 2020).

Due to its chemical composition, austenite exhibits a certain degree of instability. Consequently, manufacturing processes involving plastic deformation mechanisms can result in the development of SIM- α' microstructures in stainless steels. Extensive investigations have been conducted on forming SIM- α' (body-centered cubic - BCC) in these steels, as it plays a significant role in suppressing crack initiation and propagation during straining, leading to improved mechanical properties (MARTELO; MATEO; CHAPETTI, 2015). This transformation can occur directly from austenite to α' martensite or through an intermediate phase known as epsilon martensite (ϵ), which acts as a precursor to alpha martensite (α') (CASTAÑEDA *et al.*, 2021). The quantity of ϵ martensite decreases as the amount of α' martensite increases, as ϵ martensite is a source for α' nucleation one. This transformation process from austenite to martensite is crucial for strengthening austenitic stainless steel during straining. However, twinning mechanisms may also exist, competing with martensite formation (GALINDO-NAVA; RIVERA-DÍAZ-DEL-CASTILLO, 2017).

The instability of austenite is often described in the literature in terms of stacking fault energy (SFE), which primarily depends on the steel's chemical composition (CASTAÑEDA *et al.*, 2021). The predominant hardening mechanisms, either SIM- α' formation or mechanical twinning, are determined by SFE values. The Transformation Induced Plasticity (TRIP) effect is associated with the appearance of α' martensite, while the Twinning Induced Plasticity (TWIP) effect occurs due to mechanical twinning during austenite straining. An 18 mJ/m² SFE value threshold is commonly cited for martensitic transformation (ALLAIN *et al.*, 2004). Below this value, SIM- α' growth is the dominant mechanism, while twinning becomes the primary mechanism above this value. An empirical expression widely used to estimate the SFE value for commercial austenitic steels based on their chemical composition is represented by **Equation 1** (SCHRAMM; REED, 1975):

$$SFE \left(\frac{mJ}{m^2} \right) = -53 + 6.2 (\%Ni) + 0.7 (\%Cr) + 3.2 (\%Mn) + 9.3 (\%Mo) \quad (1)$$

Another crucial parameter influencing martensitic transformation is the straining temperature. Lower temperatures result in a higher amount of SIM- α' formation when comparing the same strain levels. Literature also indicates a continuous decrease in SFE with decreasing temperature, which can be modeled using **Equation 2** (GALINDO-NAVA; RIVERA-DÍAZ-DEL-CASTILLO, 2017):

$$SFE_{cryogenic} \left(\frac{mJ}{m^2} \right) = SFE_{RT} + 0.05 (T - 273) \quad (2)$$

Here, T represents the test temperature in kelvin.

This study aims to contribute little to understanding the influence of straining temperature on the mechanical and microstructural behavior of AISI 304 austenitic stainless steel, establishing correlations between temperature, strain levels, and the amount of SIM- α' .

MATERIAL

The material used in this study was AISI 304 austenitic stainless steel, received in the annealed state and commercially available as a sheet. The chemical composition of the steel is shown in **Table 1**.

Table 1 - Chemical composition of AISI 304 austenitic stainless steel studied, obtained using an optical emission spectrometer. The values are expressed in weight percentages (wt. %)

Chemical Composition (wt. %)									
C	Mn	Si	P	S	Cr	Ni	Mo	Others	Fe
0.044	1.255	0.550	0.040	0.018	17.665	8.100	0.140	1.339	bal.

Source: Own authorship.

Chemical composition measurements were obtained using an Ametek Spectromaxx optical emission spectrometer located at the Laboratory of Characterization and Processing of Metals (CPM) in the National Laboratory for Nanotechnology (LNNano) at the National Center for Energy and Materials Research (CNPEM). Based on the steel's chemical composition, the SFE value was estimated to be 14.9 mJ/m² at room temperature, according to **Equation 1**. The SFE value for cryogenic temperature was calculated to be 5.9 mJ/m², according to **Equation 2**. These are expected values for AISI 304 austenitic stainless steel under studies conditions (GALINDO-NAVA; RIVERA-DÍAZ-DEL-CASTILLO, 2017; SCHRAMM; REED, 1975).

OPTICAL MICROSCOPY

The as-received AISI 304 stainless steel samples underwent a series of preparation steps for metallographic analysis. Initially, the samples were ground using 2400-grit abrasive paper and mechanical polishing with 0.25 μm colloidal silica. Subsequently, electrolytic polishing was conducted using an Eletromet 4 electrolytic polishing system from Buehler®. The electrolyte used for this process consisted of a mixture of 40% anhydrous sulfuric acid in 60% anhydrous methanol (320 mL of sulfuric acid + 480 mL of methanol) at a voltage of 12 V for 60 seconds. After the electrolytic polishing, an electrolytic etching step (1st etch) was performed, followed by a chemical etching step (2nd etch). For the 1st etch, an electrolytic mixture of 60% anhydrous HNO_3 in distilled water was used, applying a voltage between 1.1 V and 2 V for 180 seconds to emphasize austenite grain boundaries. The 2nd etch utilized Beraha II solution, composed of 80 mL of water, 20 mL of HCl, and 0.3 g of potassium metabisulfite. The immersion time for the 2nd etch started from 30 seconds and aimed to etch the microstructure resulting from straining (SIM- α' or shear bands). Although optical microscopy has been used in literature to quantify SIM- α' (TALONEN, J.; ASPEGREN; HÄNNINEN, 2004), it is worth noting that SIM- α' is very thin (AGUIAR *et al.*, 2019) and undistinguishable from shear bands at the magnifications provided by optical microscopy, needing Transmission Electron Microscopy to show details (DAS *et al.*, 2008; TALONEN, JUHO *et al.*, 2005). Therefore, in this study, the evolution of the microstructure was only qualitatively analyzed, and no phase quantification was performed using optical microscopy.

MICROHARDNESS MEASUREMENTS

Microhardness measurements were performed using a Leco LM 100AT Vickers microhardness tester with a 1 kg load (HV 1) applied for 15 seconds for each measure. Fifteen hardness measurements were taken within the applicable zone of each sample (percentage of strain), and the variability of the obtained data was represented by error bars on the graph. These tests were conducted at the Laboratory of Characterization and Processing of Materials (CPM), affiliated with the National Laboratory for Nanotechnology (LNNano) at the National Center for Energy and Materials Research (CNPEM).

FERRITESCOPE MEASUREMENTS

Magnetic measurements were performed using a Helmuth Fischer FMP30 ferritescope on each strained sample. In the case of strained austenitic steels, a correction needs to be applied to the measured value (F) to estimate the amount of SIM- α' ($c_{\alpha'}$), according to **Equation 3** (TALONEN, JUHO *et al.*, 2005):

$$c_{\alpha'} = 1.71 x (F) \quad (3)$$

The measurements were plotted as a function of true strain (ϵ_t). The true strain is a function of engineering strain (ϵ) obtained using **Equation 4** (TALONEN, JUHO *et al.*, 2005):

$$\epsilon_t = \ln(1 + \epsilon) \quad (4)$$

These tests were conducted at the Laboratory of Characterization and Processing of Materials (CPM), affiliated with the National Laboratory for Nanotechnology (LNNano) at the National Center for Energy and Materials Research (CNPEM).

SIM- α' TRANSFORMATION RATE

The SIM- α' transformation rate can be determined by calculating the derivative of the transformed fraction for true strain vs. true strain ($df_{\alpha'}/d\epsilon_t \times \epsilon_t$) (QUITZKE *et al.*, 2021; TSUCHIDA *et al.*, 2013). This analysis helps determine the range of straining where the highest transformation rate occurs and establish correlations with mechanical behavior.

COMPLETE STRESS-STRAIN CURVE

Complete mechanical tests were performed until fracture on one sample at room temperature ($298 \text{ K} \pm 1 \text{ K}$) and the other at cryogenic temperature ($93 \text{ K} \pm 1 \text{ K}$), obtaining stress-strain curves for each condition. The tests were conducted using a Gleeble 3550 machine installed at the XRD1 experimental station of the Brazilian Synchrotron Light Laboratory (LNLS), part of CNPEM. From these tests, mechanical behavior parameters such as yield strength, ultimate tensile strength, and uniform elongation can be obtained.

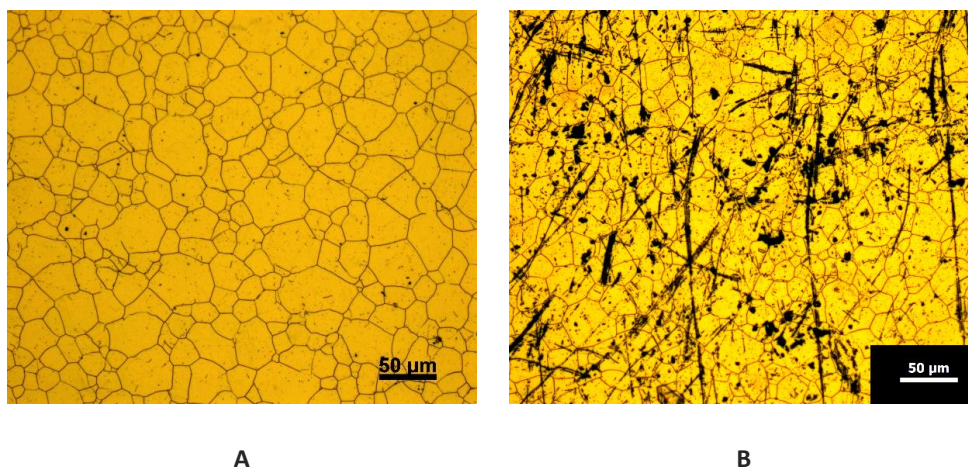
RESULTS AND DISCUSSION

Based on the conducted experiments, the obtained results are described as follows.

MICROGRAPH ANALYSIS

After the preparation step, the first electrolytic etch was performed to show the austenitic grains. Subsequently, a chemical etching was carried out in the same sample to etch residual δ -ferrite. The resulting micrographs for the as-received (undeformed) sample are shown in **Figure 2A** and **Figure 2B**.

Figure 2 - Micrographs of the as-received sample of AISI 304 austenitic stainless steel. In A, after electrolytic etch with 60% anhydrous HNO_3 in distilled water, applying approximately 2 V for 180 seconds, revealing austenite grain boundaries. In B, immersion etch with Beraha II etchant for about 30 seconds, etching δ -ferrite. Magnification is indicated by the scale bar



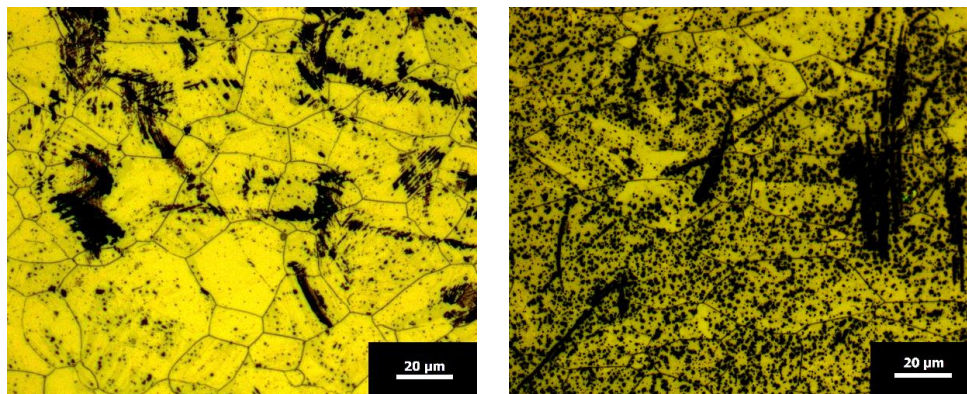
Source: Own authorship.

By observing **Figure 2A**, it can be seen that the austenitic grains are reasonably equiaxed. In **Figure 2B**, dark points and streaks stained by the Beraha II etchant can be observed. It indicates that the as-received sample has a surface with residual δ -ferrite, resulting from the chemical composition and manufacturing process (CRIVOI *et al.*, 2020). **Figures 3A** and **3B** show the evolution of the steel's microstructure after straining at room temperature (298 K). Similarly, **Figure 4A** and **Figure 4B** show the evolution of the steel's microstructure after testing at cryogenic temperature (93 K). The samples were subjected to double metallographic etching (electrolytic and chemical, as described in the previous section).

By comparing **Figure 3A** and **Figure 3B** with **Figure 2B** (undeformed sample), it can be observed that straining leads to an increase in the dark regions. It means that, qualitatively, in addition to the initial material's δ -ferrite content, straining introduces shear bands and SIM- α' .

Figure 3 - Micrographs of the AISI 304 austenitic stainless steel samples strained at room temperature (298 K), using double etching, with final Beraha II etching for approximately 30 seconds. In A, the strain is 0.125 mm/mm, and in B, the strain is 0.875 mm/mm.

Austenite appears as a bright region



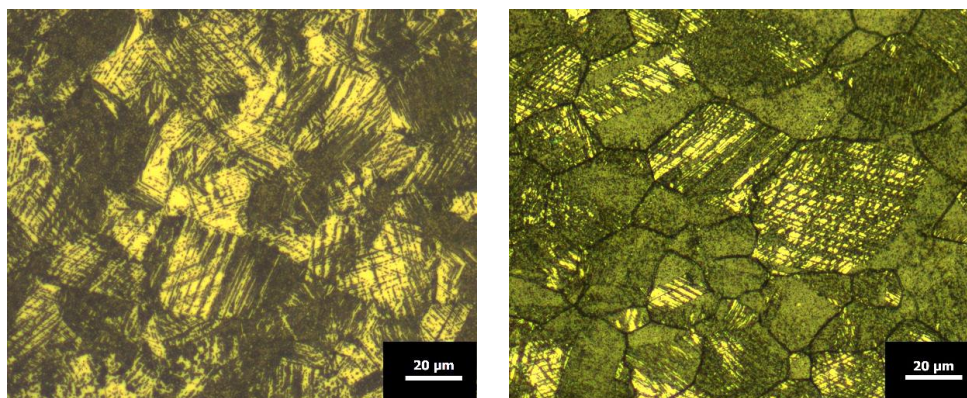
A

B

Source: Own authorship.

Figure 4 - Micrographs of the AISI 304 austenitic stainless steel samples strained at cryogenic temperature (93 K), using double etching, with final Beraha II etching for approximately 30 seconds. In A, the strain is 0.125 mm/mm, and in B, 0.875 mm/mm.

Austenite appears as a bright region



A

B

Source: Own authorship.

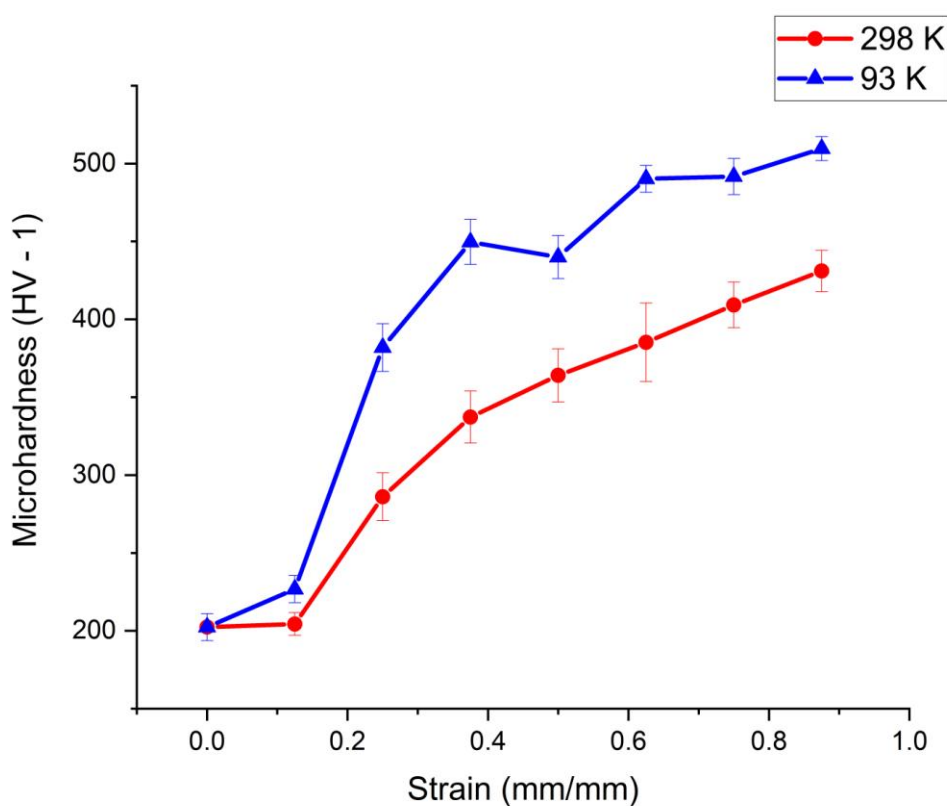
Similarly, comparing **Figures 4A** and **4B** with **Figure 2B** (undeformed sample), it can be observed that straining leads to an increase in the dark regions. By comparing **Figures 3** (A and B) and **4** (A and B), it is noted that the samples strained at 93 K have a more significant amount of dark zones for the same strain level, suggesting a higher amount of shear bands and SIM- α' (QUITZKE *et al.*, 2021). As described in the methods, this study did not perform phase quantification by optical microscopy since SIM- α' is a very thin and small phase. Even with coalescence, it is indistinguishable from shear bands, so the

micrographs were just used as a qualitative means to evaluate the strained material (AGUIAR *et al.*, 2019; DAS *et al.*, 2008; TALONEN, JUHO *et al.*, 2005).

HARDNESS MEASUREMENTS

Figure 5 shows the hardness profile as a function of engineering straining (mm/mm) for austenitic stainless steel AISI 304 at room (298 K) and cryogenic (93 K) temperatures.

Figure 5 – Vickers microhardness of austenitic stainless steel AISI 304 strained at various straining levels at ambient (298 K) and cryogenic (93 K) temperatures



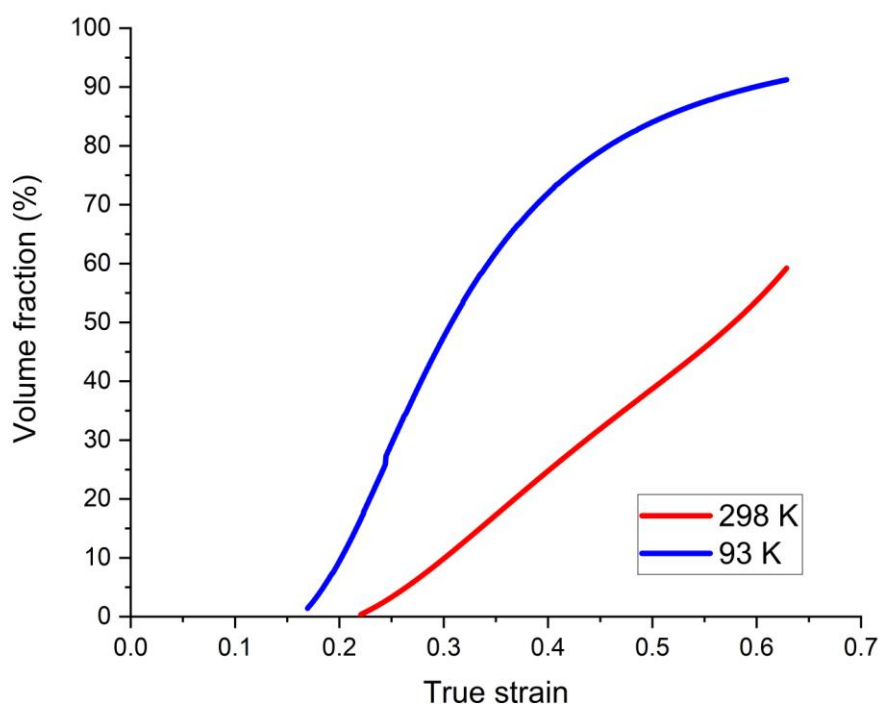
Source: Own authorship.

It is possible to observe that the hardness increases gradually with the growth of the straining level. It is still observed that hardening is higher in the sample strained at cryogenic temperature (93 K). This greater hardness at cryogenic temperature may be related to the partial suppression of dynamic recovery at low temperatures and the more significant amount of SIM- α' , as qualitatively observed in Figures 3 and 4 (CRIVOLI *et al.*, 2020).

FERRITESCOPIY

SIM- α' in austenitic stainless steel has a body-centered cubic (BCC) crystalline structure and displays ferromagnetic behavior. Consequently, the presence of α' martensite upon straining the steel leads to changes in the sample's magnetic measurements, enabling the estimation of its volume fraction through ferritescopy. The obtained SIM- α' quantities through ferritescopy, along with the corresponding measures corrected according to **Equation 3**, are illustrated in **Figure 6**, as already reported in the literature (TALONEN, J.; ASPEGREN; HÄNNINEN, 2004; TALONEN, JUHO *et al.*, 2005).

Figure 6 – Volume fraction of SIM- α' as a function of true straining for samples strained at room temperature (298 K) and cryogenically (93 K)



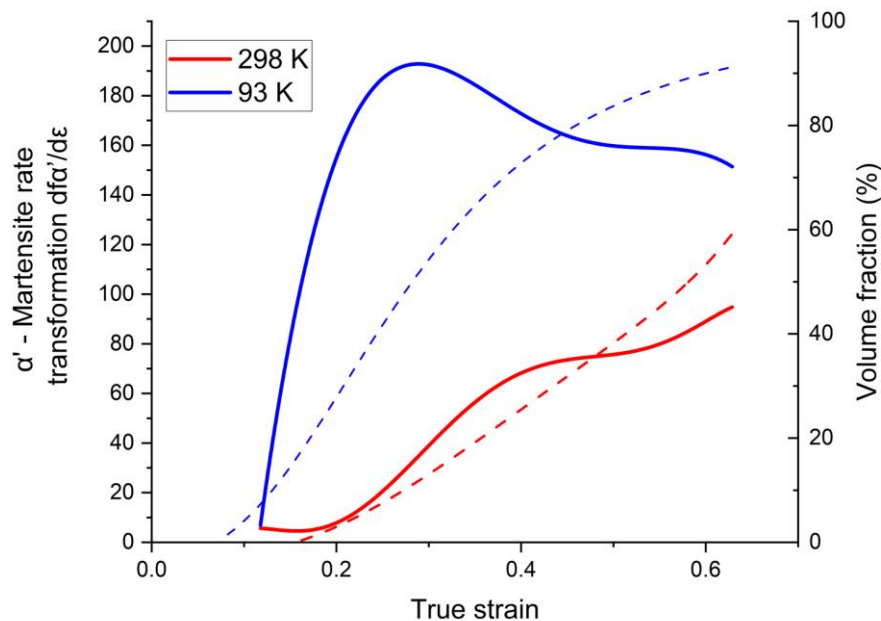
Source: Own authorship.

It is observed that the SIM- α' volume fraction increases gradually with increasing strain. In the sample strained at a temperature of 93 K, the curve has a sigmoidal shape, and the formation of SIM- α' starts at lower values of true strain (0.12) when compared with the strain at 298 K (0.22). Furthermore, for a true strain of 0.63, the SIM- α' amount reaches nearly 96% at 93 K, while only around 60% at 298 K. The SIM- α' formation is dependent on the SFE, which depends on the temperature. The SFE (5.9 mJ/m²) is smaller at 93 K than the SFE at 298 K (14.9 mJ/m²); according to **Equations 1** and **2**, then, the more straightforward transformation was expected in the cryogenic condition (93 K).

SIM- α' TRANSFORMATION RATE

Figure 7 shows the SIM- α' transformation rate ($df_{\alpha'}/d\varepsilon_t$) vs. true strain (ε_t).

Figure 7 – SIM- α' transformation rate ($df_{\alpha'}/d\varepsilon_t$) vs. true strain (ε_t) (solid lines). The dotted lines represent the SIM- α' volume fraction for comparative purposes. The graph shows the data for the room (298 K) and cryogenic (93 K) temperatures



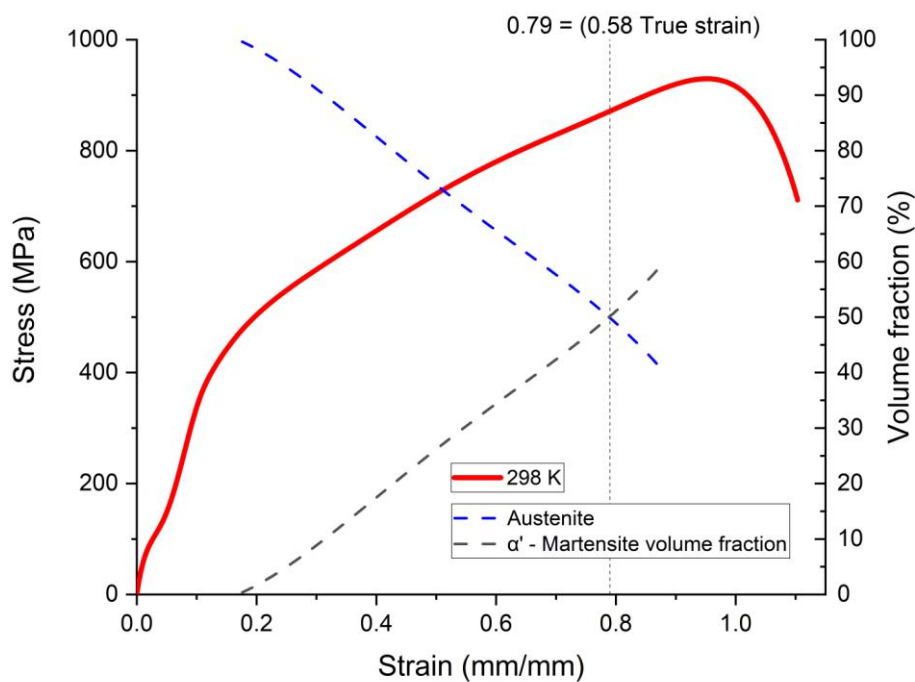
Source: Own authorship.

It is evident from **Figure 7** that the transformation rates of SIM- α' are higher at cryogenic temperature (93 K) compared to room temperature (298 K). At 93 K, a transformation peak occurs at a true strain of 0.28, coinciding with a 50% SIM- α' transformation. Conversely, at room temperature, the SIM- α' formation rate increases slowly with the strain level, and a 50% transformation is only achieved at a true strain of 0.58. At room temperature, the notable occurrence of dynamic recovery phenomena competes with SIM- α' conversion. The partial suppression of dynamic recovery likely contributes to the heightened transformation rate observed at 93 K. Additionally, this increased SIM- α' transformation rate at cryogenic temperature explains the greater observed hardening illustrated in **Figure 5** (CRIVOI *et al.*, 2020).

STRESS-STRAIN CURVES

Figure 8 and **Figure 9** show the mechanical behavior in the engineering stress-strain test of AISI 304 steel strained at room (298 K) and cryogenic (93 K) temperatures, respectively.

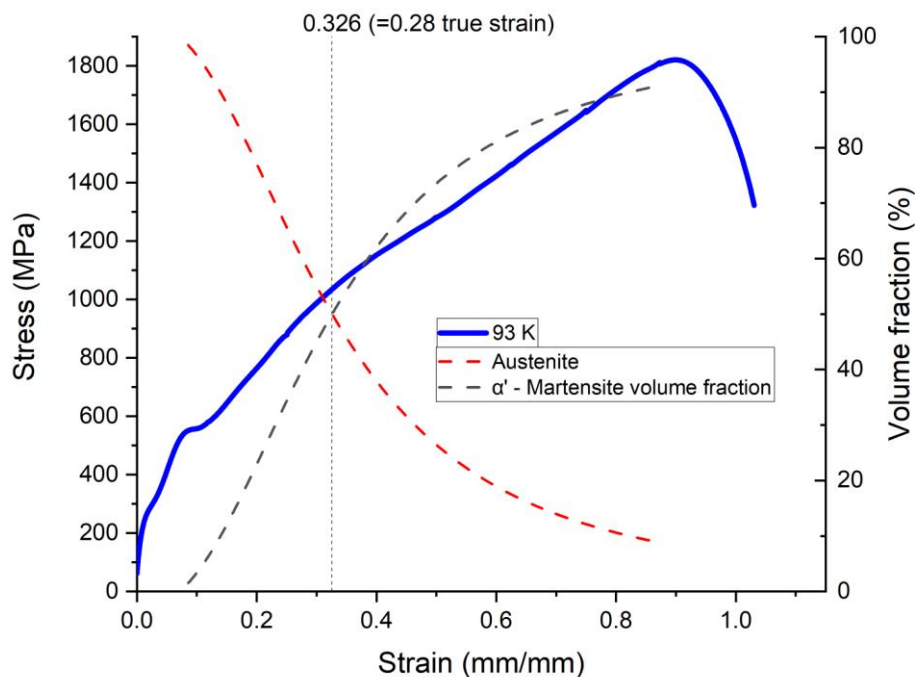
Figure 8 – Engineering stress-strain curve of AISI 304 stainless steel strained at room temperature (298 K). The scale on the right also represents the SIM- α' formation as a function of engineering strain



Source: Own authorship.

In **Figure 8**, it is possible to observe a plastic region with a gradual increase in stress as a function of straining. On the scale on the right, it can be seen that the SIM- α' fraction reaches 50% in the final stages of straining 0.79 mm/mm (equivalent to 0.58 true strain).

Figure 9 – Engineering stress-strain curve of AISI 304 stainless steel strained at cryogenic temperature (93 K). The scale on the right also represents the SIM- α' formation as a function of engineering strain



Source: Own authorship.

By analyzing **Figure 9**, it is possible to observe a plastic region with a greater increase in stress due to straining. On the scale on the right, it can be seen that the SIM- α' fraction reaches 50% in the initial stages of straining 0.326 mm/mm (equivalent to 0.28 true strain). The amount of SIM- α' formed in the cryogenic straining is much higher at the end of the test (60% higher). Thus, when comparing Figures 8 and 9, it is observed that with cryogenic straining, there are higher yield strength and tensile strength limits without significant loss of elongation. **Table 2** summarizes some parameters obtained in this work.

The literature states that the decrease in temperature promotes a reduction in SFE, and lower SFE values increase the instability of austenite (GALINDO-NAVA; RIVERA-DÍAZ-DEL-CASTILLO, 2017). This statement aligns with our findings, as the material strained at 93 K, with an engineering straining of 0.875 mm/mm, forms 60% more martensite compared to the material performed under the same conditions at 298 K. It is noteworthy that cryogenic straining (93 K) triples the yield strength, nearly doubles the tensile strength, and decreases the uniform elongation by only 4.3% compared to room temperature straining (298 K). These phenomena may be partly associated with the partial suppression of dynamic recovery at low temperatures and the more significant amount of SIM- α' formed, related to the TRIP effect (CRIVOI *et al.*, 2020; SOHRABI *et al.*, 2023).

Table 2 - Summary of mechanical strength parameters obtained in this work

Parameter	298 K (RT.)	93 K (cryogenic)	Variation (%)
Yield strength (MPa)	183	558	+ 205
tensile strength (MPa)	930	1820	+96
Uniform elongation(mm/mm)	0.93	0.89	-4.3
SIM- α' volume fraction at the end of the test (%)	60	96	+60
SFE (mJ/m ²)*	14.9	5.9	-60

Source: Own authorship.

* obtained by Equations 1 and 2

CONCLUSIONS

This study investigated AISI 304 austenitic stainless steel straining at room (298 K) and cryogenic (93 K) temperatures. Based on the results and discussion, the following conclusions can be drawn:

The microhardness increases gradually with the increase in the level of strain. This increase is more pronounced in the cryogenic condition. The austenite in this steel transforms SIM- α' during straining. Ferritescope's measurements revealed that for the same strain level, there are higher amounts of SIM- α' in the cryogenically strained sample. Higher transformation rates also occur under cryogenic conditions. In the measurement performed with straining of 0.875 mm/mm, the volume fraction of SIM- α' is 96% at cryogenic temperature and 60% at room temperature. The stress-strain curves show that under cryogenic conditions, the yield strength increases by 205%, and the tensile strength increases by 96%, with no significant loss in uniform elongation, only 4.3%. The higher values of mechanical strength parameters under cryogenic conditions can be attributed to the partial suppression of dynamic recovery and the higher content of SIM- α' , which is associated with the TRIP effect.

Efeito da temperatura na deformação do aço inoxidável austenítico AISI 304

RESUMO

O estudo examinou a influência da deformação plástica no aço inoxidável austenítico AISI 304 em temperaturas ambiente (298 K) e criogênica (93 K). Inicialmente, foram realizadas sete amostras em diferentes níveis de deformação de engenharia (0,125, 0,25, 0,375, 0,5, 0,625, 0,75, 0,875 mm/mm) em ambas as temperaturas. Os resultados foram comparados com uma amostra não deformada, no estado como recebido. A análise da evolução da microestrutura envolveu técnicas como microscopia óptica, medições de microdureza e ferritoscopia. Posteriormente, foram realizados ensaios mecânicos completos até que a amostra rompesse em cada temperatura, gerando curvas tensão-deformação. Esses experimentos foram realizados utilizando o Sistema de Simulação Termomecânica (XTMS) localizado na estação experimental XRD1 do Laboratório Nacional de Luz Síncrotron (LNLS) do Centro Nacional de Pesquisa em Energia e Materiais (CNPEM). Os resultados indicaram que a quantidade de martensita α' induzida por deformação (MID- α') aumentou com o nível de deformação, principalmente em amostras realizadas em baixas temperaturas. Em uma deformação de engenharia de 0,875 mm/mm, a quantidade de MID- α' atingiu 96% a 93 K, enquanto atingiu apenas 60% à temperatura ambiente nos mesmos níveis de deformação. Além disso, a deformação criogênica resultou em maiores taxas de transformação de MID- α' e maiores valores de microdureza. Ademais, a deformação criogênica levou a um aumento significativo na resistência ao escoamento (205% maior) e na resistência à tração (96% maior), com uma diminuição mínima no alongamento uniforme (4,3% menor) em comparação com a deformação à temperatura ambiente. Estes efeitos foram atribuídos à supressão parcial da recuperação dinâmica e à transformação da austenita em MID- α' . Os resultados sugerem a ocorrência do efeito de Plasticidade Induzida por Transformação (TRIP), contribuindo para a melhoria da resistência mecânica. Este estudo demonstrou que a deformação em temperaturas criogênicas induz mudanças favoráveis nas propriedades mecânicas do aço inoxidável austenítico, transformando a austenita em SIM- α' e inibindo a recuperação dinâmica.

PALAVRAS-CHAVE: tensão-deformação; austenita; martensita induzida por deformação.

Efecto de la temperatura en la deformación del acero inoxidable austenítico AISI 304

RESUMEN

El estudio examinó la influencia de la deformación plástica en el acero inoxidable austenítico AISI 304 a temperatura ambiente (298 K) y criogénica (93 K). Inicialmente, se realizaron siete muestras en diferentes niveles de deformación de ingeniería (0.125, 0.25, 0.375, 0.5, 0.625, 0.75, 0.875 mm/mm) a ambas temperaturas. Sus resultados se compararon con una muestra no deformada tal como se recibió, y el análisis de la evolución de la microestructura involucró técnicas como microscopía óptica, mediciones de microdureza y ferritescopia. Posteriormente se realizaron pruebas mecánicas completas hasta que la muestra falló en cada temperatura, generándose curvas tensión-deformación. Estos experimentos se realizaron utilizando el Sistema de Simulación Termomecánica (XTMS) ubicado en la estación experimental XRD1 dentro del Laboratorio Nacional de Luz Sincrotrón (LNLS) del Centro Nacional de Investigaciones en Energía y Materiales (CNPEM). Los hallazgos indicaron que la cantidad de martensita α' inducida por deformación (MID- α') aumentaba con el nivel de deformación, particularmente en muestras realizadas a bajas temperaturas. Con una deformación de ingeniería de 0.875 mm/mm, la cantidad de MID- α' alcanzó el 96 % a 93 K, mientras que solo alcanzó el 60 % a temperatura ambiente en las mismas condiciones. Además, el filtrado criogénico dio como resultado mayores tasas de transformación de MID- α' y mayores valores de microdureza. Además, la deformación criogénica condujo a un aumento significativo en el límite elástico (205% más) y la resistencia a la tracción (96% más), con una disminución mínima en el alargamiento uniforme (4.3% menos) en comparación con la deformación a temperatura ambiente. Estos efectos se atribuyeron a la supresión parcial de la recuperación dinámica y la transformación de austenita en MID- α' . Los resultados sugieren la aparición del efecto de Plasticidad Inducida por Transformación (TRIP), contribuyendo a la mejora de la resistencia mecánica. Este estudio demostró que la deformación a temperaturas criogénicas induce cambios favorables en las propiedades mecánicas del acero inoxidable austenítico al transformar la austenita en MID- α' e inhibir la recuperación dinámica.

PALABRAS-CLAVE: tensión-deformación; austenita; martensita inducida por deformación.

ACKNOWLEDGMENTS

This research was supported by Fundação Araucária and Coordenação de Aperfeiçoamento de Pessoal de Nível Superior (CAPES, Brazil). This research used facilities of the Brazilian Synchrotron Light Laboratory (LNLS), part of the Brazilian Center for Research in Energy and Materials (CNPEM), a private non-profit organization under the supervision of the Brazilian Ministry for Science, Technology, and Innovations (MCTI). The XRD1 beamline staff and CPM/CNPEM team are acknowledged for their assistance during the experiments.

REFERENCES

- AGUIAR, D. J. M. *et al.* Comparative study on the forming and reversion of strain-induced martensite in two duplex stainless steels: Developing a model for VSM analysis of powders or fine chips. *Journal of Magnetism and Magnetic Materials*, v. 485, p. 8–15, 1 set. 2019.
- ALLAIN, S. *et al.* Correlations between the calculated stacking fault energy and the plasticity mechanisms in Fe-Mn-C alloys. *Materials Science and Engineering A*, v. 387–389, n. 1- 2 SPEC. ISS., p. 158–162, 15 dez. 2004.
- CASTAÑEDA, J. A. *et al.* Stacking fault energy determination in fe-mn-al-c austenitic steels by x-ray diffraction. *Metals*, v. 11, n. 11, 1 nov. 2021.
- CELADA-CASERO, C. *et al.* In-situ investigation of strain-induced martensitic transformation kinetics in an austenitic stainless steel by inductive measurements. *Metals*, v. 7, n. 7, 13 jul. 2017.
- CRIVOI, M. R. *et al.* In situ analysis of cryogenic strain of AISI 316L stainless steel using synchrotron radiation. *Cryogenics*, v. 105, 1 jan. 2020.
- DAS, A. *et al.* Morphologies and characteristics of deformation induced martensite during tensile deformation of 304 LN stainless steel. *Materials Science and Engineering A*, v. 486, n. 1–2, p. 283–286, 15 jul. 2008.
- GALINDO-NAVA, E. I.; RIVERA-DÍAZ-DEL-CASTILLO, P. E. J. Understanding martensite and twin formation in austenitic steels: A model describing TRIP and TWIP effects. *Acta Materialia*, v. 128, p. 120–134, 15 abr. 2017.
- MARTELO, D. F.; MATEO, A. M.; CHAPETTI, M. D. Fatigue crack growth of a metastable austenitic stainless steel. *International Journal of Fatigue*, v. 80, p. 406–416, 13 jul. 2015.

MAXIMOV, J. *et al.* Effects of Heat Treatment and Diamond Burnishing on Fatigue Behaviour and Corrosion Resistance of AISI 304 Austenitic Stainless Steel. *Applied Sciences (Switzerland)*, v. 13, n. 4, 1 fev. 2023.

QUITZKE, C. *et al.* Evaluation of strain-induced martensite formation and mechanical properties in N-alloyed austenitic stainless steels by in situ tensile tests. *Materials Science and Engineering A*, v. 808, 18 mar. 2021.

SCHRAMM, R. E.; REED, R. P. Stacking fault energies of seven commercial austenitic stainless steels. *Metallurgical Transactions A*, v. 6, n. 7, p. 1345–1351, jul. 1975.

SOHRABI, M. J. *et al.* Grain size dependent mechanical behavior and TRIP effect in a metastable austenitic stainless steel. *International Journal of Plasticity*, v. 160, 1 jan. 2023.

TALONEN, J.; ASPEGREN, P.; HÄNNINEN, H. Comparison of different methods for measuring strain induced α' -martensite content in austenitic steels. *Materials Science and Technology*, v. 20, n. 12, p. 1506–1512, dez. 2004.

TALONEN, JUHO *et al.* Effect of strain rate on the strain-induced $\gamma \rightarrow \alpha'$ -martensite transformation and mechanical properties of austenitic stainless steels. *Metallurgical and Materials Transactions A*, v. 36, n. 2, p. 421–432, fev. 2005.

TSUCHIDA, N. *et al.* Effects of temperature and strain rate on trip effect in SUS301L metastable austenitic stainless steel. *ISIJ International*, v. 53, n. 10, p. 1881–1887, 2013.

Recebido: 12 de junho de 2023.
Aprovado: 6 de outubro de 2023.

DOI:

Como citar: DE AGUIAR, D J M; FONTANA, H O; DE AGUIAR, D B S; SENRA, A L T; IZUMI, M T; WU, L; CARVALHO, A M G; CINTHO, O M, Effect of temperature on straining of AISI 304 austenitic stainless steel, *Revista Brasileira de Física Tecnológica Aplicada*, Ponta Grossa, v. 10, n. 2, p. 1-18, dez. 2023.

Contato: Denilson José Marcolino de Aguiar: denilsonaguiar@utfpr.edu.br

Direito autoral: Este artigo está licenciado sob os termos da Licença Creative Commons-Atribuição 4.0 Internacional.

